NANO EXPRESS

Effects of architectures and H_2O_2 additions on the photocatalytic performance of hierarchical Cu_2O nanostructures

Xiaolong Deng[*], Qiang Zhang, Qinqin Zhao, Lisha Ma, Meng Ding and Xijin Xu[*]

Abstract

Cu_2O hierarchical nanostructures with different morphologies were successfully synthesized by a solvothermal method using copper (II) nitrate trihydrate ($Cu(NO_3)_2 \cdot 3H_2O$) and ethylene glycol (EG) as initial reagents. The obtained nanostructures were characterized by X-ray diffraction (XRD), scanning electron microscopy (SEM), Brunauer-Emmett-Teller (BET) specific surface area test, and UV-vis spectroscopy. The synthesis conditions (copper source, temperature, and reaction time) dominated the compositions and the formation of crystals with different morphologies. The visible light photocatalytic properties of as-prepared Cu_2O nanostructures were investigated with and without hydrogen peroxide (H_2O_2), and the effect of H_2O_2 were evaluated by monitoring the degradation of methyl orange (MO) with various amounts of H_2O_2. It was revealed that the degree of the photodegradation of MO depends on the amount of H_2O_2 and the morphology of Cu_2O.

Keywords: Cu_2O; Hierarchical nanostructures; Photocatalytic properties; H_2O_2; Visible light

Background

Over the past decades, the remarkable developments of industry have induced environmental pollution which has become one of the most critical issues for the future sustainable development [1-3]. Therefore, considerable attention has been paid to fabricate photocatalytic materials with high efficiency and low cost to solve environmental problem. Metal oxide nanostructures with desired architectures have become promising candidates due to their unique properties and potential applications in many fields [4-6]. Among these metal oxides, cuprous oxide (Cu_2O) has attracted considerable interest due to the wide applications in the fields of lithium-ion batteries [7], solar energy conversion [8,9], optical limiter [10], gas sensor [11,12], storage device [13,14], and catalysis [15,16]. Furthermore, its bandgap of 1.9 to 2.2 eV endowing them absorb visible light of solar spectrum [17], and the optical bandgaps can be fine-tuned by changing the size of nanoparticles [13], which is very helpful to degrade dye pollutants. Moreover, Cu_2O was first explored for water splitting under visible light irradiation in 1998 [18].

Since then, many efforts have been made to investigate the factors influenced on the photocatalytic activities, and the applications have also been extended to the photodegradation of dye pollutants [3,19-23].

Since the photocatalytic activities could be strongly affected by the structural and morphological characters of materials including size, shape, and exposed crystalline plane [21,24], many approaches have been suggested to fabricate photocatalytic materials, such as chemical vapor deposition [25], hybrid laser processing and chemical dealloying [21], chemical transformation [10], electrochemical deposition [23], thermal decomposition [3], aqueous colloidal solution approach [26], and hydrothermal route [20]. Through these methods, varied shapes of Cu_2O micro/nano-structures have been successfully synthesized, including nanowire polyhedrals [20], microcrystalline particle films [24], polyhedral microparticles [27], nanocages (nanoframes) [13,28], hollow octahedrals [29], hollow spheres [29], nanocubes [2,30], nanoplates [31], and nanoboxes [32].

In addition, hydrogen peroxide (H_2O_2) plays an important role in the photocatalytic activities of Cu_2O on the degradation of dye pollutants, acting as an electron and hydroxyl radical ($OH^\bullet$) scavenger which prevents the

* Correspondence: sps_dengxl@ujn.edu.cn; sps_xuxj@ujn.edu.cn
School of Physics and Technology, University of Jinan, 336 NanxinZhuang West Road, Jinan 250022, Shandong Province, Peoples Republic of China

Springer

Deng *et al. Nanoscale Research Letters* (2015) 10:8

Page 2 of 9

recombination of electron-hole pairs generated during the catalysis [3,20,29]. However, there are only a few reports that investigated the effect of H_2O_2 amount on the degradation of dye based on Cu_2O crystalline particle films [23,24], and almost no reports based on Cu_2O nanoparticles. Furthermore, controversies exist about the direct photodegradation of dyes by Cu_2O materials in the absence of H_2O_2 [20,27]. Therefore, we carried out the research in order to overall understand the effect of H_2O_2 on the photocatalytic activities of Cu_2O particles and to clarify the controversies of Cu_2O for direct photodegradation of dyes.

In this report, we investigated the effects of synthesis conditions on the structural and morphological features by growing Cu_2O nanostructures through solvothermal approach. The effect of H_2O_2 amount on the photocatalytic activities of Cu_2O materials was systematically studied. It was demonstrated that the compositions of the products and the formation of crystals with different morphologies could be greatly affected by the synthesis conditions. It was also revealed that the presence of different amounts of H_2O_2 and different Cu_2O nanoarchitectures would play important roles in the photodegradation of methyl orange (MO).

Methods

All the chemical reagents, purchased from Sinopharm Chemical Reagent Co., Ltd. (SCRC, China), were of analytical grade and used without further purification. The synthesis conditions used in this work are listed in Table 1. For the synthesis of Cu_2O nanostructures, a typical procedure (S1 to S4 in Table 1) was as follows, according to the previous report [33]: $Cu(NO_3)_2 \cdot 3H_2O$ (4 mmol, 0.9664 g) was dissolved in 80 mL ethylene glycol under vigorous stirring, then the mixture was transferred into 100 mL Teflon-lined stainless steel autoclave. After that, the autoclave was sealed and placed into oven at 140°C for several hours. Subsequently, the autoclave was cooled down to room temperature naturally. The obtained precipitants were centrifuged and washed with deionized water and ethanol several times. The final products were collected by drying the precipitants in a vacuum oven at 60°C for 12 h.

X-ray powder diffraction (XRD) patterns were carried out to analyze the crystallographic structures of the products on a German X-ray diffractometer (D8-Advance, Bruker AXS, Inc., Madison, WI, USA) equipped with Cu $K\alpha$ radiation ($\lambda = 0.15406$ nm). The morphologies of the products were observed by a field emission scanning electron microscopy (FESEM; FEI QUANTA FEG250, FEI, Hillsboro, USA). The Brunauer-Emmett-Teller (BET) specific surface areas of the products were investigated by N_2 adsorption isotherm at 77 K using a full-automatic specific surface analyzer (3H-2000BET-A, Beishide Instrument, Beijing, China).

The morphology-related photocatalytic activities of as-prepared Cu_2O nanostructures were performed with a UV-vis spectrophotometer (TU-1901, Beijing Purkinje General Instrument Co., Ltd, Beijing, China) under visible light irradiation at ambient temperature in air. The visible light was generated by a 500 W Xe lamp equipped with a cutoff filter to remove the UV part with wavelength below 420 nm. In a typical procedure, 20 mg/L MO solution was prepared by dissolving 10 mg MO in 500 mL deionized water, then 30 mg of products was added into 50 ml of as-prepared MO solution in a quartz bottle to form a suspension. Prior to illumination, the suspension was kept in dark for 30 min with stirring to reach adsorption-desorption equilibrium of MO on the surface of the Cu_2O nanostructures. Then, different amounts of H_2O_2 (30 wt%) aqueous solution were added into the suspension before turning on the light. Ca. 3 mL of the dye aqueous solution was taken out at a given irradiation time interval and centrifuged to filtrate the sample powders. The concentration of the dye (MO) aqueous solution was measured by testing the absorbance properties at 464 nm in UV-vis spectra. The degradation rate of MO was defined as follows [24]:

Table 1 The synthesis conditions used for the preparation of Cu_2O nanostructures

Sample	Copper source	Ethylene glycol (mL)	Temperature (°C)	Time (h)
S1	4 mmol $Cu(NO_3)_2 \cdot 3H_2O$	80	140	4
S2	4 mmol $Cu(NO_3)_2 \cdot 3H_2O$	80	140	6
S3	4 mmol $Cu(NO_3)_2 \cdot 3H_2O$	80	140	8
S4	4 mmol $Cu(NO_3)_2 \cdot 3H_2O$	80	140	10
S5	4 mmol $Cu(CH_3COO)_2 \cdot H_2O$	80	140	10
S6	4 mmol $Cu(CH_3COO)_2 \cdot H_2O$	80	160	12
S7	4 mmol $Cu(CH_3COO)_2 \cdot H_2O$	80	180	6
S8	4 mmol $Cu(NO_3)_2 \cdot 3H_2O$	80	180	6
S9	4 mmol $Cu(NO_3)_2 \cdot 3H_2O$	80	140	3
S10	8 mmol $Cu(CH_3COO)_2 \cdot H_2O$	80	160	12

Deng *et al. Nanoscale Research Letters* (2015) 10:8

Page 3 of 9

$$\text{degradation rate} = \frac{C_o - C}{C_o} \times 100\%$$

where C_0 and C are the absorbance value at 464 nm in UV-vis spectra before and after a given time interval of the degradation of MO, respectively.

The optical absorption behaviors of the synthesized samples were investigated by measuring UV-vis absorbance spectra directly through dissolving powders into ethanol.

Results and discussion

Figure 1 shows the XRD patterns of as-prepared products (S1 to S4) obtained at different reaction time. All the peaks of XRD patterns from S2 to S4 can be indexed by ICCD-JCPDS database (card no. 78-2076), which demonstrate that the as-prepared products are the pure Cu_2O with a cubic symmetry. For the sample S1, the XRD pattern can also be indexed to the cubic Cu_2O; however, there is a peak around 43.3° being indexed to cubic Cu (111) peak (JCPDS no. 85-1326), which meant that the as-prepared product (S1) is impure Cu_2O. The average Cu_2O crystallite size of samples S1 to S4 were calculated to be 11.7 nm (S1), 13.8 nm (S2), 17.4 nm (S3), and 22.3 nm (S4), respectively, by the Debye-Scherer formula combining with Jade 5 software [15,22]. For investigating the effect of reaction time on the phases of obtained products, sample S9 was carried out; however, no precipitant was collected, the final solution kept blue color as the original solution. Thus, reaction time could dominate the phase and control the average crystallite size of the as-prepared samples. Figure 2 depicts the XRD patterns obtained from S5 to S8 and S10 at different temperature and copper sources. Compared the patterns of S5 in Figure 2 and S4 in Figure 1, S4 was
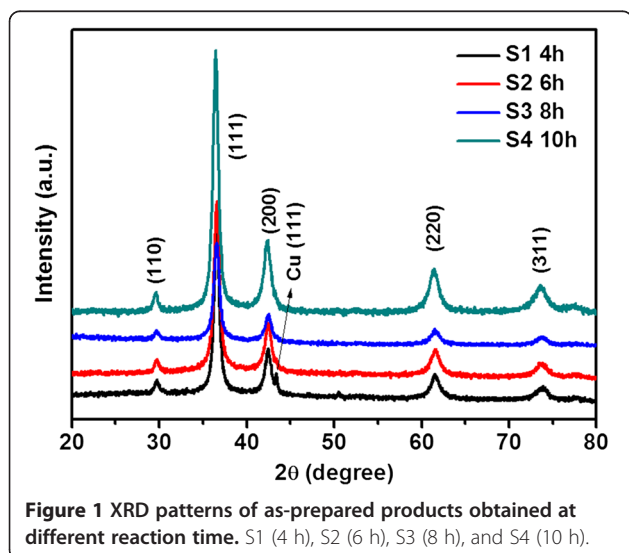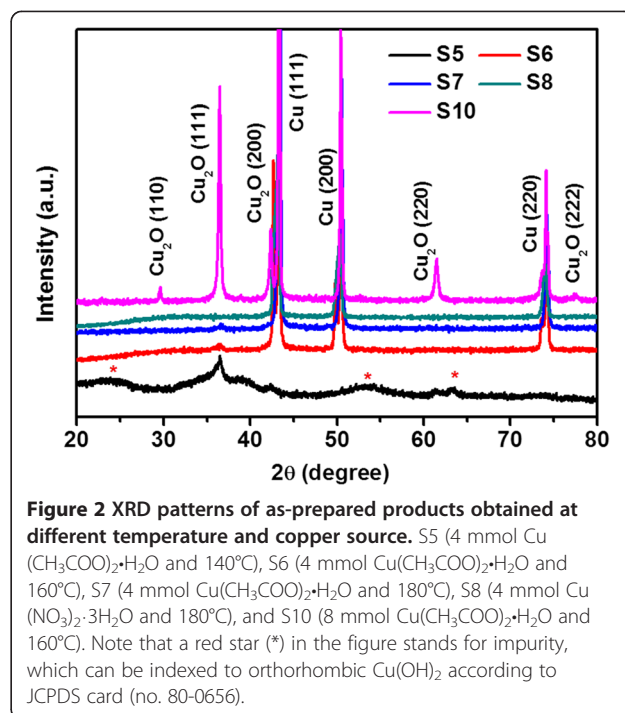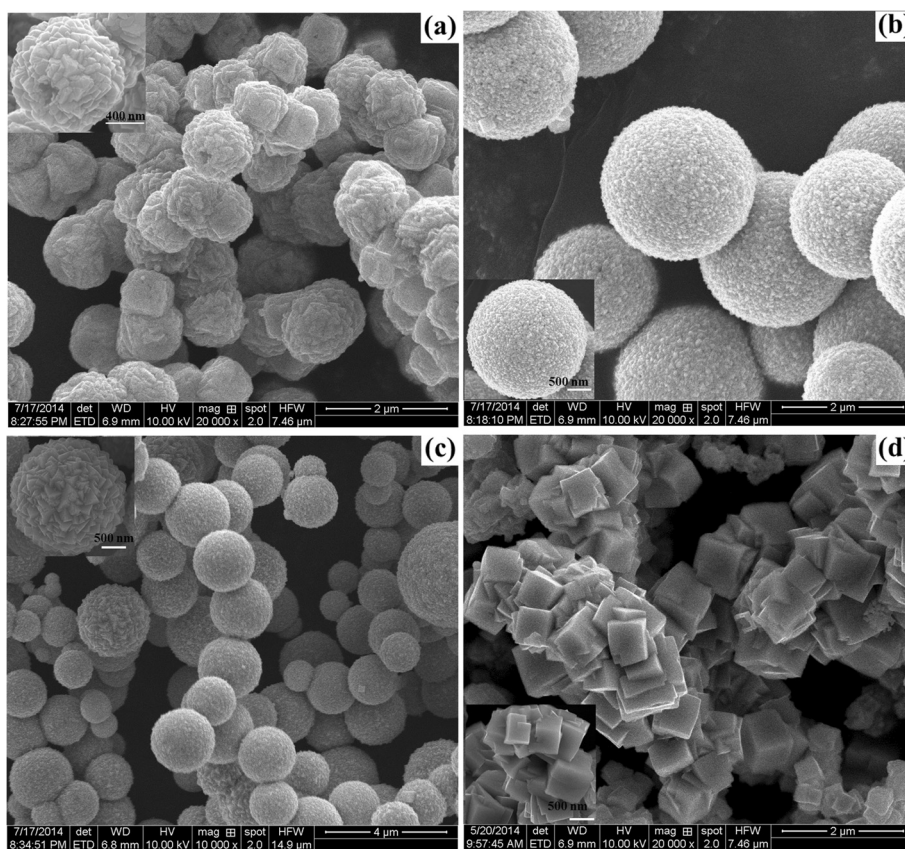

Figure 2 XRD patterns of as-prepared products obtained at different temperature and copper source. S5 (4 mmol Cu $(CH_3COO)_2 \cdot H_2O$ and 140°C), S6 (4 mmol $Cu(CH_3COO)_2 \cdot H_2O$ and 160°C), S7 (4 mmol $Cu(CH_3COO)_2 \cdot H_2O$ and 180°C), S8 (4 mmol Cu $(NO_3)_2 \cdot 3H_2O$ and 180°C), and S10 (8 mmol $Cu(CH_3COO)_2 \cdot H_2O$ and 160°C). Note that a red star (*) in the figure stands for impurity, which can be indexed to orthorhombic $Cu(OH)_2$ according to JCPDS card (no. 80-0656).

pure Cu_2O while S5 was impure Cu_2O with poor crystallization, which illustrated that the phase of obtained product was varied when the copper source was changed. With the temperature increasing from 140°C to 180°C (sample S5, S6, and S7), the compositions experienced an evolution from Cu_2O with impurity (S5), Cu_2O mixing with Cu (S6), and pure Cu (S7). Pure Cu was also obtained at 180°C (S8) when 4 mmol $Cu(NO_3)_2 \cdot 3H_2O$ was used as copper source. Therefore, temperature played an important role in the composition of as-synthesized products. The influence of copper source amount was also studied by comparing S6 with S10. The composition was not changed ($Cu_2O + Cu$), but the ratio of Cu_2O/Cu increased. In a word, the synthesis conditions, including copper source, temperature, and reaction time, have significant influence on the phases of as-prepared products.
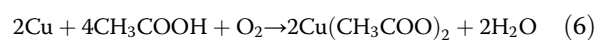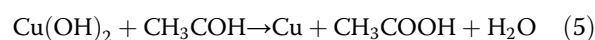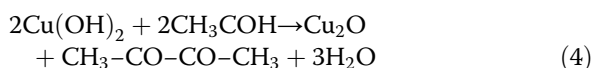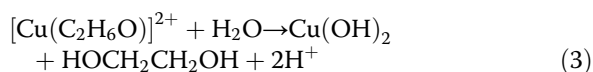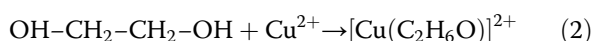
The morphologies of as-prepared samples S1 to S4 under different reaction time are observed by SEM, as shown in Figure 3. The spherical-like crystals were observed with size of 0.5 to 1 μm in Figure 3a for sample S1, which was synthesized at reaction time of 4 h. As increasing reaction time to 6 h, the spherical crystals with rough surface were obtained, as shown in Figure 3b, with the size dispersion of 0.6 to 2.5 μm, which was larger than that of 4 h reaction time. From the inset magnified SEM image, it was easy to find that the sphere was composed of large amount of pyramid particles with diameter of 50 to 100 nm. Figure 3c displays similar morphology as Figure 3b, with the larger spheres of 0.8 to 3.5 μm composing of tremendous pyramids with size

Figure 1 XRD patterns of as-prepared products obtained at different reaction time. S1 (4 h), S2 (6 h), S3 (8 h), and S4 (10 h).

Deng *et al. Nanoscale Research Letters* (2015) 10:8

Page 4 of 9

Figure 3 SEM images of the as-obtained products fabricated at 140°C with different reaction time. (a) 4 h (S1), **(b)** 6 h (S2), **(c)** 8 h (S3), and **(d)** 10 h (S4) (insets are the corresponding magnified SEM images).

of 250 to 300 nm, when the reaction time was further extended to 8 h. As the reaction time reached 10 h, the morphology was completely changed to hierarchical structure consisted of cubic particles with size of 300 to 600 nm, as shown in Figure 3d. The SEM results confirmed that the reaction time had strong influence on the morphological and structural characters of as-obtained products, which were consistent with the calculation from XRD data.

Based on the aforementioned results, we proposed the growth mechanism as follows. For the use of $Cu(NO_3)_2 \cdot 3H_2O$ as copper source, the possible chemical reactions occurred in the system as follows [33,34]:

$$OHCH_2CH_2OH \rightarrow CH_3COH + H_2O \quad (1)$$

$$OH-CH_2-CH_2-OH + Cu^{2+} \rightarrow [Cu(C_2H_6O)]^{2+} \quad (2)$$

$$[Cu(C_2H_6O)]^{2+} + H_2O \rightarrow Cu(OH)_2 \\ + HOCH_2CH_2OH + 2H^+ \quad (3)$$

$$2Cu(OH)_2 + 2CH_3COH \rightarrow Cu_2O \\ + CH_3-CO-CO-CH_3 + 3H_2O \quad (4)$$

$$Cu(OH)_2 + CH_3COH \rightarrow Cu + CH_3COOH + H_2O \quad (5)$$

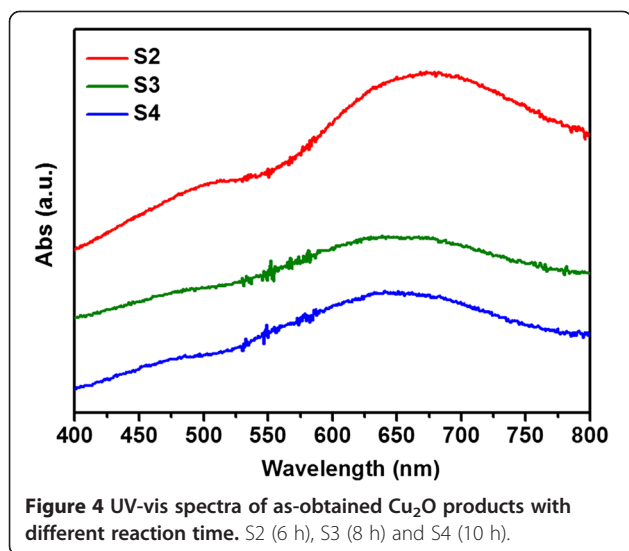$$2Cu + 4CH_3COOH + O_2 \rightarrow 2Cu(CH_3COO)_2 + 2H_2O \quad (6)$$

Therefore, the reaction listed in Equation 5 would occur for the short time under the suitable temperature, while Equation 6 would happen as more time were needed to dissolve Cu in this system. Herein, Cu phase was contained in the product. For the reactions with longer time (such as S2, S3, and S4), the reactions (Equation 1, 2, 3, 4, 5, and 6) sufficiently occurred and only Cu_2O phase existed in the products because enough time was supplied to dissolve Cu like Equation 6. However, the higher reaction temperature up to 180°C induced the reaction final stop at the stage of Equation 5; therefore, the final products were pure Cu phase. When $Cu(CH_3COO)_2 \cdot H_2O$ is used as copper source, the aforementioned reactions will occur, but the Cu phase will always appear under higher temperature due to the slow decomposition speed.

As mentioned in previous reports [33,34], spheres are easier to be formed according to the coordinate adsorption, oriented attachment and Ostwald ripening route

Deng *et al. Nanoscale Research Letters* (2015) 10:8

Page 5 of 9

under solvothermal conditions. In brief, Cu^{2+} ions can be easily formed to a relatively stable complex $[Cu(II)EG]^{2+}$ by chelating reagent ethylene glycol (EG), followed by the slow transformation into $Cu(OH)_2$ precursors due to the different stability constants and the sharp decrease of free Cu^{2+} ion concentration, resulting in the separation of nucleation and growth steps. Then, $Cu(OH)_2$ could be reduced to Cu_2O by the acetaldehyde molecules generated from the dehydration of EG. The freshly unstable Cu_2O pyramids tend to assemble oriented attachments into large spheres driven by the minimization of interfacial energy. As the reaction time increases, the small Cu_2O pyramids grow larger and change into cubes, and the spheres are broken to form hierarchical structures. Therefore, the temperature plays an important role in the control of compositions of products as well as copper source affects the compositions of products a little bit, while the reaction time has an effective influence on the morphology evolution of products.

The optical absorption behaviors were investigated by UV-vis absorbance spectra, as shown in Figure 4. The optical bandgaps could be affected by the synthetic conditions which are in good agreement with Zhang's report [35]. The strong light scattering bands resulted from the sizes of the samples, which were observed dominantly in the absorption spectra for the samples S2, S3 and S4, similar to the previous report [26]. These light scattering bands and absorption bands show progressive blue shifts with the increase of the size for S2, S3, and S4. The bandgap energy (E_g) calculated from the absorption at 450 to 525 nm is in the range of 2.36 to 2.76 eV, which is consistent with other reports [17,22,26]. The values greater than that of bulk Cu_2O at 2.17 eV are attributed to the quantum confinement effects [22,26]. These results confirmed that the as-prepared

**Figure 4** UV-vis spectra of as-obtained Cu_2O products with different reaction time. S2 (6 h), S3 (8 h) and S4 (10 h).

Cu_2O products were suitable candidates for photocatalysts under visible range of the solar spectrum.

Figure 5 shows the photocatalytic activities of as-obtained Cu_2O products without H_2O_2 additions (UV-vis spectral variations of MO in an aqueous solution were shown in Additional file 1: Figure SI-1). It is found from Figure 5A that the concentrations of MO decrease continually with an increase of irradiation duration under visible light for samples S1 to S4 with Cu_2O products while MO is kept almost no change for the pure MO solution. The different ratios of MO degradation are also observed which can be attributed to the morphology difference. The pseudo-first-order kinetics model was used to determine the rate constant of photodegradation of MO with respect to the degradation time [3,6]:

$$ln\,(C/C_0) = -kt$$

where $C0$ is the initial concentration of MO and C is the concentration at time t, k is the reaction rate constant. The plots of $ln(C/C0)$ versus time t for MO degradation using Cu_2O products were illustrated in Figure 5B. The rate constants were given by the slopes of linear lines and estimated to be 0.031 min^{-1}, 0.0214 min^{-1}, 0.00985 min^{-1}, and 0.00651 min^{-1} for samples S1, S2, S3, and S4, respectively. The obtained values demonstrated that the degradation rates for MO followed the order of S1 > S2 > S3 > S4 without the addition of H_2O_2. The degradation rate can reach 93% without the addition of H_2O_2, which is higher than other reports such as Cu_2O nanoparticles [3], Cu_2O microcrystals [27], Cu_2O-graphene [36], and pure CuO microsphere and CuO/Cu_2O microspheres [37].

The effects of H_2O_2 amount on the photocatalytic activities are presented in Figure 6. The UV-vis absorption spectra of MO in an aqueous solution with different amount of H_2O_2 and in the presence of Cu_2O products with different reaction time were shown in Additional file 1: FigureSI-2, SI-3, and SI-4. The degradation rate of 86% was observed with 40 μL H_2O_2 which is higher than other reports such as Cu_2O nanoparticles [3], $Cu_2O/$ CuO hollow microspheres [38], micro-nanohierarchical Cu_2O structure [21], and Cu_2O microcrystalline particle film [24]. For samples S1 (Figure 6A) and S2 (Figure 6B), the photocatalytic activities were inhibited when the amount of H_2O_2 were increased from 0 μL to 1,000 μL. However, for samples S3 (Figure 6C) and S4 (Figure 6D), the different behaviors were observed compared with S1 and S2. For sample S3 (8 h), the photodegradation rate with the addition of 40 μL H_2O_2 achieved maximum, as shown in Figure 6C, which is the same to sample S4. There is no obvious difference with increase of the amounts of H_2O_2. On the other hand, the effects of reaction time were also investigated on the photodegradation

Deng *et al. Nanoscale Research Letters* (2015) 10:8

Page 6 of 9
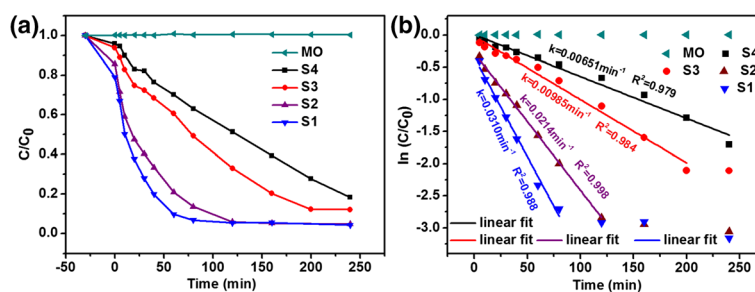
Figure 5 Photocatalytic activity of as-obtained Cu₂O products under visible light. (a) Plots of concentration ratios of MO in an aqueous solution against given irradiation intervals in the presence or absence of Cu₂O products for samples S1 to S4, which depicted the synthesis conditions as listed in Table 1. **(b)** The plots of ln(C/C_0) versus time of MO degradation in presence of Cu₂O products, without H₂O₂.
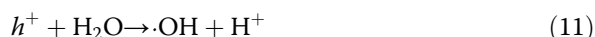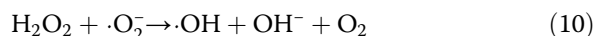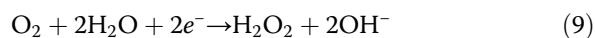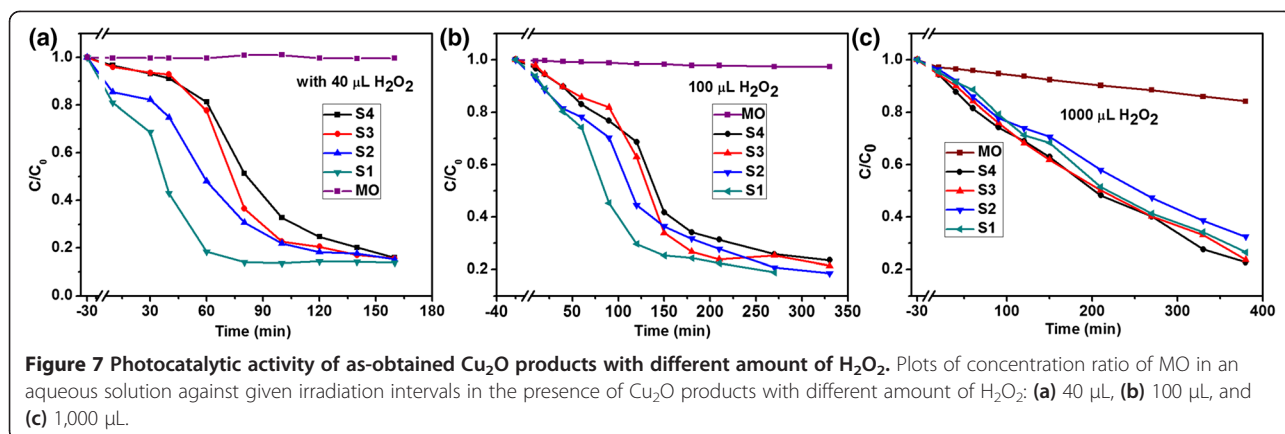
of MO in an aqueous solution with different amounts of H₂O₂, as shown in Figure 7. The corresponding curves of ln($C/C0$) versus time t for MO degradation using Cu₂O products were plotted in Additional file 1: FigureSI-5. Combining with Figure 5A, the gap of the effect of reaction time on the photodegradation rate was rapidly closing when the amount of H₂O₂ was increased, which meant that the morphology effect on the photocatalytic activity became weaker by increasing the addition of H₂O₂ amount. The results are slightly different from the previous reports [23,24], which can be attributed to the competition between the effect of H₂O₂ and the morphology of Cu₂O photocatalysts. That means H₂O₂ plays a dominant

role in the process of photodegradation when a mass of H₂O₂ and lager-sized photocatalysts are used.

The mechanism of a possible photochemical reaction was proposed according to the factors influenced on the photocatalytical activity. The electron can excite from valence band (VB) to conductance band (CB) under visible light irradiation to the surface of Cu₂O, as shown in Equation 1, and thus, a series of reactions could be induced by the photogenerated electrons and holes as follows [23,24,29,39]:

$$Cu_2O + h\nu \rightarrow e^- (CBCu_2O) + h^+ (VBCu_2O) \qquad (7)$$

$$O_2 + e^- \rightarrow \cdot O_2^- \qquad (8)$$
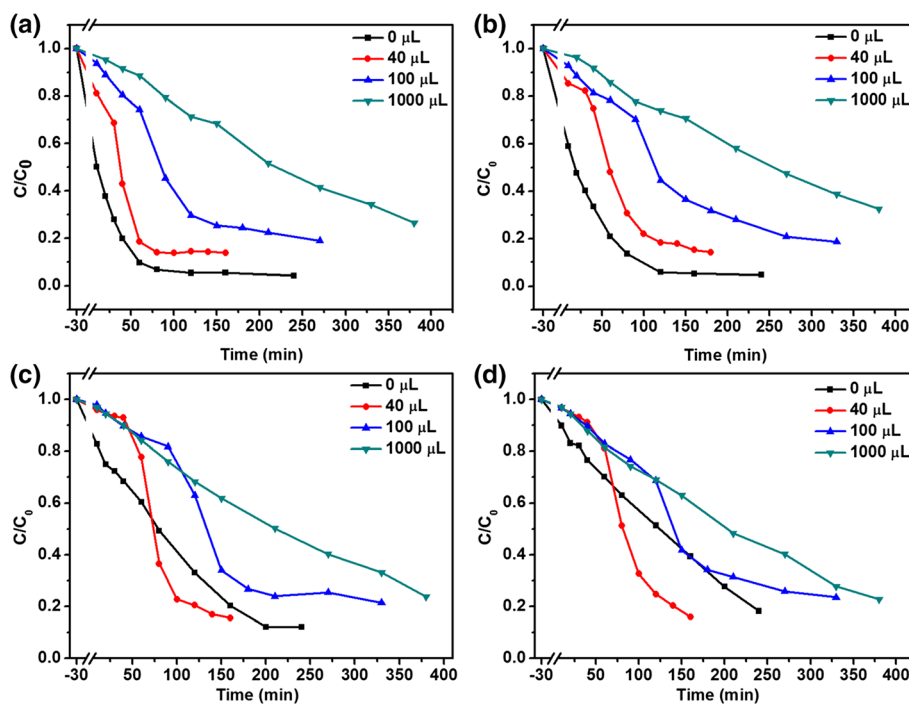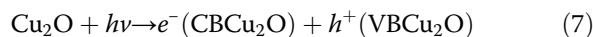
Figure 6 Photodegradation of MO in an aqueous solution with Cu₂O products and different amount of H₂O₂. (a) 4 h (S1), **(b)** 6 h (S2), **(c)** 8 h (S3), and **(d)** 10 h (S4).

Deng *et al. Nanoscale Research Letters* (2015) 10:8

Page 7 of 9

Figure 7 Photocatalytic activity of as-obtained Cu₂O products with different amount of H₂O₂. Plots of concentration ratio of MO in an aqueous solution against given irradiation intervals in the presence of Cu₂O products with different amount of H₂O₂: **(a)** 40 μL, **(b)** 100 μL, and **(c)** 1,000 μL.

$$O_2 + 2H_2O + 2e^- \rightarrow H_2O_2 + 2OH^- \qquad (9)$$

$$H_2O_2 + \cdot O_2^- \rightarrow \cdot OH + OH^- + O_2 \qquad (10)$$

$$h^+ + H_2O \rightarrow \cdot OH + H^+ \qquad (11)$$

$$\cdot OH + MO \rightarrow \text{degradation products} \qquad (12)$$

For the degradation of MO in the presence of Cu₂O without the addition of H₂O₂ as shown in Figure 5A, the photocatalytic reaction can be as follows based on the previous report [21,23]: First, the photogenerated electrons and holes were formed under visible irradiation of Cu₂O, as depicted in Equation 7; Secondly, the electrons were scavenged by oxygen (O₂) to generate superoxide ions (O_2^-) (Equation 8) and H₂O₂ (Equation 9). Then, O_2^- reacted with H₂O₂ to produce hydroxyl radicals (•OH) (Equation 10). The holes reacted also with H₂O to produce hydroxyl radicals (•OH), as displayed in Equation 11. Finally, the pollutants (MO) were oxidized into inorganic or nontoxic products by hydroxyl radicals (•OH) (Equation 12). The difference of photodegradation rate of samples S1 to S4 could be ascribed to the morphological character [39,40]. It was well known that the surface area and surface state strongly affected the activity of photocatalyst due to the photocatalytic reaction always taking place at the surface of photocatalyst [39,40]. The specific surface area of as-obtained Cu₂O products were evaluated to be 8.44 m²/g, 5.50 m²/g, 4.68 m²/g, and 5.07 m²/g for samples S1, S2, S3, and S4 (as shown in Additional file 1: Figure SI-7 and Table SI-1). Although the total surface area of sample S4 was higher than that of S3, the photocatalytic activity of S4 lower, which may be ascribed to more [111] surface on sample S3 [29]. Another reason may be ascribed to the difference of bandgap, the bandgap energies (E_g) calculated from the absorption at 450 to 525 nm are in the range of 2.36 to 2.76 eV for samples S2, S3, and S4, which means that more photogenerated electrons and holes occur on the surfaces of samples with the order of S2 > S3 > S4 for the same irradiation

condition. Moreover, sample S1 contains a small mass of Cu, which can be identified from XRD pattern. This Cu phase may also enhance the photodegradation by promoting the rapid separation of photogenerated electrons and holes in the interfaces between Cu and Cu₂O [41,42].

Once adding H₂O₂ into the aqueous solution, the photochemical process became complicated. H₂O₂ was considered to be a good electron acceptor by numerous studies, and thus it could be converted to •OH by accepting electrons (Equation 10) [23]. Based on this view, the addition of H₂O₂ with a suitable amount should enhance the photodegradation rate which was confirmed in our experiments, as shown in Figure 6C,D, while the results in Figure 6A,B were inconsistent with this view. From Additional file 1: FigureSI-6, it can be seen that the photodegradation rate was continually enhanced by increasing of H₂O₂ in the absence of Cu₂O products for decomposition of MO in an aqueous solution, although the absolute values of photodegradation rates were very small. Therefore, both H₂O₂ and Cu₂O could enhance the photodegradation of MO in an aqueous solution as aforementioned, respectively. However, when the two products were mixed together and placed into MO solution, the photocatalytic activity was not further enhanced in some cases. This may result from the photochemical reaction between H₂O₂ and Cu₂O, as follows [23,43]:

$$2H_2O_2 \overset{Cu_2O}{\rightarrow} 2H_2O + O_2 \qquad (13)$$

$$Cu_2O + H_2O_2 \rightarrow 2CuO + H_2O, \qquad (14)$$
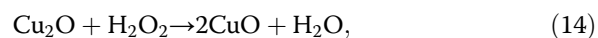
which indicated that H₂O₂ would be decomposed into O₂ by Cu₂O (Equation 13) and would react with Cu₂O to produce CuO (Equation 14) depending on the amount of H₂O₂ and the morphology of Cu₂O product. According to the previous report [44], the photocorrosion of Cu₂O will induce them changing into CuO, resulting in the loss of photogenerated charges, and herein, the photodegradation

Deng *et al. Nanoscale Research Letters* (2015) 10:8

Page 8 of 9

rate decreases. The reaction (Equation 14) preferably occurs at the surfaces of nanosized particles due to its high activity, which means the amount of H_2O_2 would affect the samples' photodegradation rate with the sequence of S1 > S2 > S3 > S4. Therefore, the final photocatalytic activity on the photodegradation of MO in an aqueous solution should be determined by both H_2O_2 and Cu_2O. As for the effects of H_2O_2, they act as inhibitor of the photodegradation for the samples with smaller size but work as activator while the photocatalysts with large size are used. Therefore, both the additive H_2O_2 and morphology of Cu_2O products played important roles in the photocatalytic activity, the final efficiency could be determined by the competition of the effect of H_2O_2 and morphology.

Conclusions

In summary, hierarchically nanostructured Cu_2O samples were successfully synthesized by a solvothermal method. The structural and morphological characters were investigated by XRD and SEM to prove that the synthesis conditions had significant influence on the composition of products and the formation of crystal with diverse morphologies. The specific surface areas of as-obtained samples were also observed to explain the difference of photodegradation rate with as-obtained samples. The amount of H_2O_2 additive was confirmed to play an important role in the photodegradation of MO as well as morphology under visible light irradiation. It was revealed that the photocatalytic activities were of comprehensive effect of the amount of H_2O_2 and the morphology of Cu_2O photocatalysts.

Additional file

Additional file 1: Supporting information. FigureSI-1, FigureSI-2, FigureSI-3, FigureSI-4, FigureSI-5, FigureSI-6, FigureSI-7, and TableSI-1.

References

1. Eltzov E, Pavluchkov V, Burstin M, Marks RS. Creation of a fiber optic based biosensor for air toxicity monitoring. Sensor Actuat B-Chem. 2011;155:859–67.
2. Zhou LJ, Zou YC, Zhao J, Wang PP, Feng LL, Sun LW, et al. Facile synthesis of highly stable and porous Cu_2O/CuO cubes with enhanced gas sensing properties. Sensor Actuat B-Chem. 2013;188:533–9.
3. Kumar B, Saha S, Ganguly A, Ganguli AK. A facile low temperature (350°C) synthesis of Cu_2O nanoparticles and their electrocatalytic and photocatalytic properties. RSC Adv. 2014;4:12043–9.
4. Rackauskas S, Nasibulin AG, Jiang H, Tian Y, Kleshch VI, Sainio J, et al. A novel method for metal oxide nanowire synthesis. Nanotechnology. 2009;20:165603.
5. Solanki PR, Kaushik A, Agrawal VV, Malhotra BD. Nanostructured metal oxide-based biosensors. NPG Asia Mater. 2011;3:17–24.
6. Zaman S, Zainelabdin A, Amin G, Nur O, Willander M. Efficient catalytic effect of CuO nanostructures on the degradation of organic dyes. J Phys Chem Solids. 2012;73:1320–5.
7. Liu WJ, Chen GH, He GH, Zhang W. Synthesis of starfish-like Cu_2O nanocrystals through γ-irradiation and their application in lithium-ion batteries. J Nanopart Res. 2011;13:2705–13.
8. Yuhas BD, Yang PD. Nanowire-based all-oxide solar cells. J Am Chem Soc. 2009;131:3756–61.
9. Wei HM, Gong HB, Chen L, Zi M, Cao BQ. Photovoltaic efficiency enhancement of Cu_2O solar cells achieved by controlling homojunction orientation and surface microstructure. J Phys Chem C. 2012;116:10510–5.
10. Gao J, Li Q, Zhao H, Li L, Liu C, Gong Q, et al. One-pot synthesis of uniform Cu_2O and CuS hollow spheres and their optical limiting properties. Chem Mater. 2008;20:6263–9.
11. Zhang H, Zhu Q, Zhang Y, Wang Y, Zhao L, Yu B. One-pot synthesis and hierarchical assembly of hollow Cu_2O microspheres with nanocrystals-composed porous multishell and their gas-sensing properties. Adv Funct Mater. 2007;17:2766–71.
12. Zhang J, Liu J, Peng Q, Wang X, Li Y. Nearly monodisperse Cu_2O and CuO nanospheres: preparation and applications for sensitive gas sensors. Chem Mater. 2006;18:867–71.
13. Lu CH, Qi LM, Yang JH, Wang XY, Zhang DY, Xie JL, et al. One-pot synthesis of octahedral Cu_2O nanocages via a catalytic solution route. Adv Mater. 2005;17:2562–7.
14. Deng XL, Hong SH, Hwang IR, Kim JS, Jeon JH, Park YC, et al. Confining grains of textured Cu_2O films to single-crystal nanowires and resultant change in resistive switching characteristics. Nanoscale. 2012;4:2029–33.
15. Zhang ZL, Che HW, Gao JJ, Wang YL, She XL, Sun J. Shape-controlled synthesis of Cu_2O microparticles and their catalytic performances in the Rochow reaction. Catal Sci Technol. 2012;2:1207–12.
16. Leng M, Liu M, Zhang Y, Wang Z, Yu C, Yang X, et al. Polyhedral 50-facet Cu_2O microcrystals partially enclosed by {311} high-index planes: synthesis and enhanced catalytic CO oxidation activity. J Am Chem Soc. 2010;132:17084–7.
17. Wu L, Tsui L, Swami N, Zangari G. Photoelectrochemical stability of electrodeposited Cu_2O films. J Phys Chem C. 2010;114:11551–6.
18. Hara M, Kondo T, Komoda M, Ikeda S, Shinohara K, Tanaka A, et al. Cu_2O as a photocatalyst for overall water splitting under visible light irradiation. Chem Commun. 1998;3:357–8.
19. Xu H, Wang W, Zhu W. Shape evolution and size controllable synthesis of Cu_2O octahedra and their morphology dependent photocatalytic properties. J Phys Chem B. 2006;110:13829–34.
20. Shi J, Li J, Huang XJ, Tan YW. Synthesis and enhanced photocatalytic activity of regularly shaped Cu_2O nanowire polyhedra. Nano Res. 2011;4:448–59.
21. Dong CS, Zhong ML, Huang T, Ma MX, Wortmann D, Brajdic M, et al. Photodegradation of methyl orange under visible light by micro-nanohierarchical Cu_2O structure fabricated by hybrid laser processing and chemical dealloying. ACS Appl Mater Inter. 2011;3:4332–8.
22. Yu Y, Zhang LY, Wang J, Yang Z, Long MC, Hu NT, et al. Preparation of hollow porous Cu_2O microspheres and photocatalytic activity under visible light irradiation. Nanoscale Res Lett. 2012;7:347.
23. Zhai W, Sun FQ, Chen W, Zhang LH, Min ZL, Li WS. Applications of Cu_2O octahedral particles on ITO glass in photocatalytic degradation of dye pollutants under a halogen tungsten lamp. Mater Res Bull. 2013;48:4953–9.
24. Wu GD, Zhai W, Sun FQ, Chen W, Pan ZZ, Li WS. Morphology-controlled electrodeposition of Cu_2O microcrystalline particle films for application in photocatalysis under sunlight. Mater Res Bull. 2012;47:4026–30.
25. Barreca D, Fornasiero P, Gasparotto A, Gombac V, Maccato C, Montini T, et al. The potential of supported Cu_2O and CuO nanosystems in photocatalytic H_2 production. Chem Sus Chem. 2009;2:230–3.

Deng *et al. Nanoscale Research Letters* (2015) 10:8

Page 9 of 9

26. Kuo CH, Huang MH. Facile Synthesis of Cu_2O nanocrystals with systematic shape evolution from cubic to octahedral structures. J Phys Chem C. 2008;112:18355–60.
27. Zhang Y, Deng B, Zhang TR, Gao DM, Xu AW. Shape effects of Cu_2O polyhedral microcrystals on photocatalytic activity. J Phys Chem C. 2010;114:5073–9.
28. Sui YM, Fu WY, Zeng Y, Yang HB, Zhang YY, Chen H, et al. Synthesis of Cu_2O nanoframes and nanocages by selective oxidative etching at room temperature. Angew Chem. 2010;122:1–5.
29. Feng LL, Zhang CL, Gao G, Cui DX. Facile synthesis of hollow Cu_2O octahedral and spherical nanocrystals and their morphology-dependent photocatalytic properties. Nanoscale Res Lett. 2012;7:276.
30. Gou L, Murphy CJ. Controlling the size of Cu_2O nanocubes from 200 to 25 nm. J Mater Chem. 2004;14:735–8.
31. Ng CHB, Fan WY. Shape evolution of Cu_2O nanostructures via kinetic and thermodynamic controlled growth. J Phys Chem B. 2006;110:20801–7.
32. Teo JJ, Chang Y, Zeng HC. Fabrications of hollow nanocubes of Cu_2O and Cu via reductive self-assembly of CuO nanocrystals. Langmuir. 2006;22:7369–77.
33. Li SK, Li CH, Huang FZ, Wang Y, Shen YH, Xie AJ, et al. One-pot synthesis of uniform hollow cuprous oxide spheres fabricated by single-crystalline particles via a simple solvothermal route. J Nanopart Res. 2011;13:2865–74.
34. Liu XY, Hu RZ, Xiong SL, Liu YK, Chai LL, Bao KY, et al. Well-aligned Cu_2O nanowire arrays prepared by an ethylene glycol-reduced process. Mater Chem Phys. 2009;114:213–6.
35. Gu YJ, Su YJ, Chen D, Geng HJ, Li ZL, Zhang LY, et al. Hydrothermal synthesis of hexagonal CuSe nanoflakes with excellent sunlight-driven photocatalytic activity. Cryst Eng Comm. 2014;16:9185–90.
36. Gao ZY, Liu JL, Xu F, Wu DP, Wu ZL, Jiang K. One-pot synthesis of graphene–cuprous oxide composite with enhanced photocatalytic activity. Solid State Sci. 2012;14:276–80.
37. Wang SL, Li PG, Zhu HW, Tang WH. Controllable synthesis and photocatalytic property of uniform CuO/Cu_2O composite hollow microspheres. Powder Technol. 2012;230:48–53.
38. Yu HG, Yu JG, Liu SW, Mann S. Template-free hydrothermal synthesis of CuO/Cu_2O composite hollow microspheres. Chem Mater. 2007;19:4327–34.
39. Huang L, Peng F, Yu H, Wang HJ. Preparation of cuprous oxides with different sizes and their behaviors of adsorption, visible-light driven photocatalysis and photocorrosion. Solid State Sci. 2009;11:129–38.
40. Thompson TL, Yates J, John T. Surface science studies of the photoactivation of TiO_2-new photochemical processes. Chem Rev. 2006;106:4428–53.
41. Zhou B, Wang HX, Liu ZG, Yang YQ, Huang XQ, Lü Z, et al. Enhanced photocatalytic activity of flowerlike Cu_2O/Cu prepared using solvent-thermal route. Mater Chem Phys. 2011;126:847–52.
42. Zhou B, Liu ZG, Zhang HJ, Wu Y. One-pot synthesis of Cu_2O/Cu self-assembled hollow nanospheres with enhanced photocatalytic performance. J Nanomater. 2014;2014:291964.
43. Song Y, Ichimura M. H_2O_2 treatment of electrochemically deposited Cu_2O thin films for enhancing optical absorption. Int J Photoenergy. 2013;2013:738063.
44. Bessekhouad Y, Robert D, Weber JV. Photocatalytic activity of Cu_2O/TiO_2, Bi_2O_3/TiO_2 and $ZnMn_2O_4/TiO_2$ heterojunctions. Catal Today. 2005;101:315–21.